ISIJ International, Vol. 48 (2008), No. 9, pp. 1165–1174

Phosphorous Partition in Dephosphorization Slag Occurring with Crystallization at Initial Stage of Solidification

Pham Khanh SON and Yoshiaki KASHIWAYA

Graduate School of Engineering, Hokkaido University, Kita 13, Nishi 8, Kita-ku, Sapporo 060-8628 Japan.

(*Received on November 21, 2007; accepted on June 18, 2008*)

Basicity and the amount of Fe_tO were investigated for their effects on the crystallization behavior of the simulated dephosphorizing slags. Twelve kinds of slags were prepared (C/S=1.0–2.5, Fe_tO=10–20 %, P_2O_5=5 %). In the present experiment, the Hot Thermocouple Technique was used to melt and quench the samples. After quenching, the microstructure of the slag and the distributions of elements were examined by SEM and EDS analysis.

The diameter of the crystal which precipitated in the sample increased with increasing basicity (C/S) and decreasing Fe_tO content. In addition, glassy regions were observed in the two samples whose Fe_tO content was 20 % and whose basicity was 1.0 or 1.5. The samples (10 % Fe_tO, 5 % P_2O_5), whose basicity was 1.0 (sample-1) precipitated as a monocalcium silicate ($CaO \cdot SiO_2$); the sample (10 % Fe_tO, 5 % P_2O_5) whose basicity was 1.5 (sample-4) precipitated as a dicalcium silicate ($2CaO \cdot SiO_2$). In higher Fe_tO (15–20 %) slags, the crystals of the solid solution between $3CaO \cdot P_2O_5$ and $2CaO \cdot SiO_2$ ((C_3P–C_2S)ss) were observed. When the amount of CaO increased from C/S=1.5 to C/S=2.5, $2CaO \cdot SiO_2$ appeared with phosphorous content, but phosphorous was not found in $CaO \cdot SiO_2$.

KEY WORDS: phosphorous partition; dephosphorization; crystallization; hot thermocouple.

1. Introduction

Recently, the demand has increased for steel products of high quality and high purity which requires a more efficient method of refining process. In the hot-metal dephosphorization (de-P) process for lower the phosphorous concentration in pig-iron, the excess amount of CaO is injected into the pig-iron to improve the efficiency of the dephosphorization reaction and minimize the refractory erosion.

The injected CaO is known to react with SiO_2 in slag to form the $2CaO \cdot SiO_2$ (C_2S) phase, into which phosphorus concentrates. However, because of the excess amount of injected CaO, the undissolved CaO (termed "free CaO") remains in the slag, which causes difficulty in recycling slag and increases the slag quantity.

To reduce the amount of steelmaking slag and the free CaO, it is necessary to increase the reaction efficiency of CaO. Several investigations have been carried out to clarify the reaction of solid CaO in a molten slag.[1–8] The process of dissolving CaO is quite complicated because the melting point changes in accordance with the CaO content. When the melting point increases, some crystal-phase precipitation occurs. The CaO content is changing continuously, along with the liquidus. This illustrates one aspect of the complications of dissolving CaO into slag: as the CaO dissolves, more precipitates due to the melting-point change.

The present study addressed one part of this complicated process through simulations using the Hot Thermocouple Technique (HTT). The artificial de-P slag was melted and quenched using the HTT. The effects of basicity and Fe_tO content on the crystallization behavior of the simulated de-P slag were investigated at the initial stage of melting.

2. Experimental

2.1. Samples

The samples were prepared by mixing the reagent-grade CaO, SiO_2, Fe_tO and P_2O_5 in the desired proportions. Twelve kinds of samples were used. The chemical compositions are shown in **Table 1**. The content of P_2O_5 was 5% in all the samples, the basicity ranged from 1.0 to 2.5 and the Fe_tO contents were 10, 15 and 20%.

The sample compositions are plotted on the ternary

Table 1. Compositions of slags.

Sample No.	CaO/SiO_2	Fe_tO (mass%)	P_2O_5 (mass%)
1	1	10%	5%
2	1	15%	5%
3	1	20%	5%
4	1.5	10%	5%
5	1.5	15%	5%
6	1.5	20%	5%
7	2	10%	5%
8	2	15%	5%
9	2	20%	5%
10	2.5	10%	5%
11	2.5	15%	5%
12	2.5	20%	5%

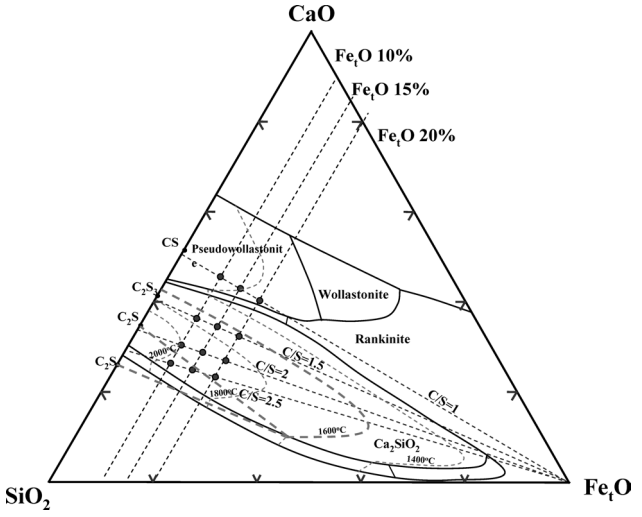

Fig. 1. Phase diagram of $CaO–SiO_2–Fe_tO$ system and compositions of samples used in this study.[9)]

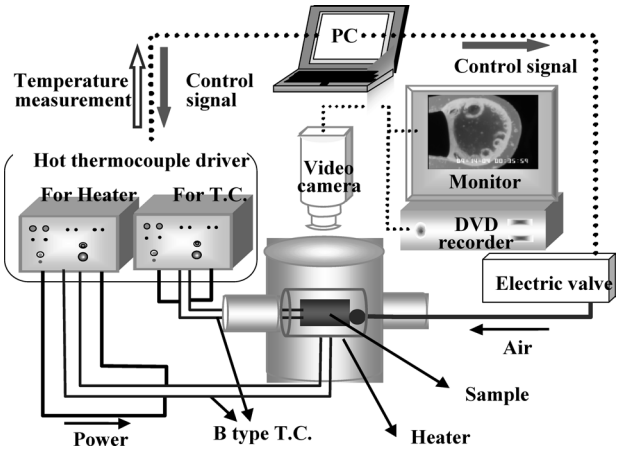

Fig. 2. Schematics of experimental apparatus.

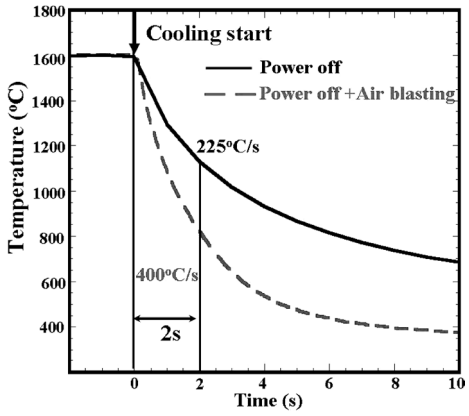

Fig. 3. Effect of air blasting on the cooling rate.

phase diagram (P_2O_5 is excluded) shown in **Fig. 1**. The initial compositions of sample-1–3 locate in the region of primary crystalline phase of monocalcium silicate (CS: $CaO \cdot SiO_2$), and the compositions of sample-4–12 locate in the region of primary crystalline phase of dicalcium silicate region (C_2S: $2CaO \cdot SiO_2$) (Fig. 1).[9)]

2.2. Experimental Apparatus

Figure 2 illustrates the experimental apparatus, which has a hot thermocouple driver and an *in situ* observation system. A small furnace was located in the reaction tube to minimize the thermal gradient in the sample, although the sample diameter was only 3 mm. The setup was newly developed based on one made by Kashiwaya *et al.* at Carnegie Mellon University.[10,11)] For rapid quenching, the air blast was carried out through the electric valve, which was synchronized with the turn-off of the electric power of the furnace and hot thermocouple. The application of the air blast could increase the cooling rate to 400 K/s (**Fig. 3**) within 2 s. The thermocouple was B-type (0.5 mmφ, Pt–30%Rh, 6%Rh) whose tip shape for melting the sample was adjusted to a given configuration (the inner tip width was 2 mm).

A powder sample was put on the thermocouple, which heated to approximately 900°C. By increasing the thermocouple temperature to 1 600°C (**Figs. 4**(a), 4(b)), the powder sample seemed to be melted instantaneously before the temperature reached to 1 600°C. Actually, in the case of the low-basicity samples (sample-1–6), the samples were melted completely (Fig. 4(2)). However, in the high-basicity sample (sample-7–12), the solid phase would form by the reaction among the powder (*ex.* $CaO+2SiO_2=2CaO \cdot SiO_2$) and the sample would be the state of coexistence of liquid and solid (Fig. 4(3)). In the present experiment, it is difficult to distinguish visually the melting of sample and the solidification start, because the crystal precipitation will be very small and occur simultaneously with the reaction of components. The details are discussed in the later Sec. 3.3.

In the present experiment, the sample was quenched just after 'melting', which means the start of solidification. The quenching procedure was started quickly, and then followed by termination of the furnace power and the application of an air blast for quenching, as mentioned above. With a high cooling rate (400 K/s), the crystallization of slag could be observed and investigated in its early stage.

The microstructure of sample and the distribution of each element were examined by using SEM and EDS.

2.3. Quantitative Analysis

In the present experiment, the quantitative analysis was carried out by EDS. The accuracy of EDS was confirmed by comparison to the results from EPMA. The details are shown in the Appendix.

3. Results and Disscusion

3.1. Crystallization Behavior of Slags

(1) Sample-1–3 (C/S=1.0, 10–20% Fe_tO, 5% P_2O_5)

Figures 5 and **6** show the results of sample-1 (C/S=1, 10% Fe_tO). Since the sample sometimes formed bubbles while melting, residual small and large bubbles are found in the quenched sample. The area near the thermocouple is glassy and the crystals are mainly observed in the center of the sample. The same phenomenon was observed in the other samples. If the welding shape of HTC were the same, the cooling ability would be the same among the different experiments. However, in the case of sample-1, the cross section of the welding site had a little gap (Fig. 5(a)) that might affect the heat conduction during cooling. As a re-

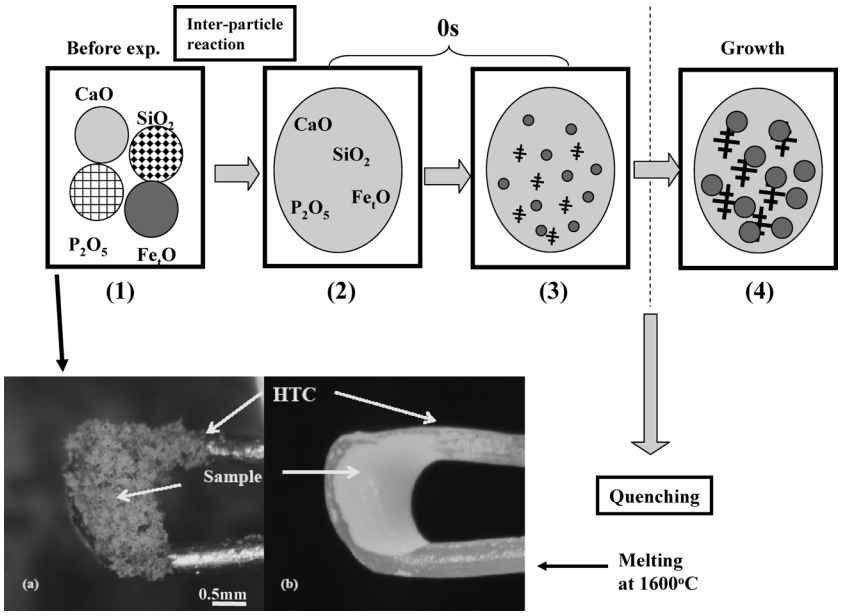

Fig. 4. Illustration of the melting of sample powder consisted of the mixture of reagent oxides and the image of melting by HTC.

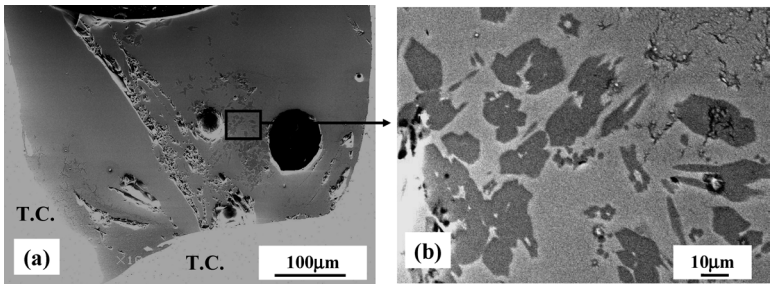

Fig. 5. SEM image of quenched slag (sample-1: C/S=1.0, 10 mass% Fe_tO, 5 mass% P_2O_5).

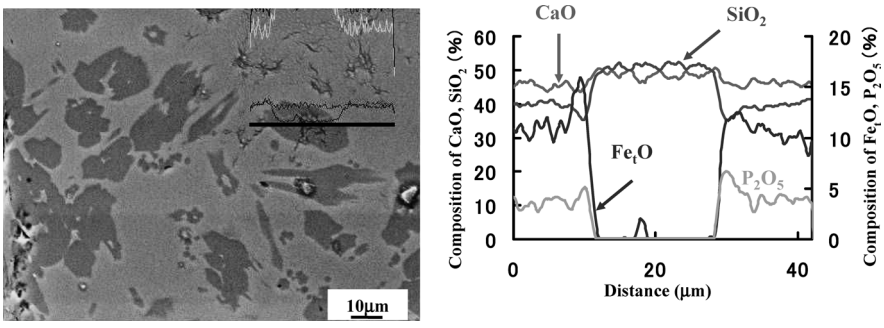

(a) (b)

Fig. 6. SEM image and line scan of quenched slag (sample-1: C/S 1.0, 10 mass% Fe_tO, 5 mass% P_2O_5).

sult, the position of the crystal area was a little different from the other samples. The crystals are 10–20 μm in length and 2–10 μm in width; some of them have the needle-like shape, characteristic of sample-1.

Figure 6(b) shows the result of line analysis on the position of precipitated crystal (Fig. 6(a)). The concentration of Fe_tO and P_2O_5 was higher in the liquid, while the concentration of CaO and SiO_2 was higher in the crystals. Since the concentrations of CaO and SiO_2 were almost the same (45–55%), the crystals are considered to be monocalcium silicate (CS). The concentration distribution of P_2O_5 indicates that the phosphorous mostly exists in the liquid phase, and does not exist in the crystals.

Sample-2 has showed the same tendency as sample-1, but sample-3 (20% Fe_tO) did not show the crystallization. The details and the reason are shown in the later sections (Secs. 3.2 and 3.3).

(2) Sample-4–6 (C/S=1.5, 10–20% Fe_tO, 5% P_2O_5)

Figure 7 shows the results of sample-4 (C/S=1.5, 10% Fe_tO). The area near the thermocouple was glassy and crystals were observed in the center area. And the dendritic structure was observed in the area between the glassy and crystalline regions. The dendritic structure seemingly grew from the crystals.

Figure 8 shows the results of EDS analysis for sample-4.

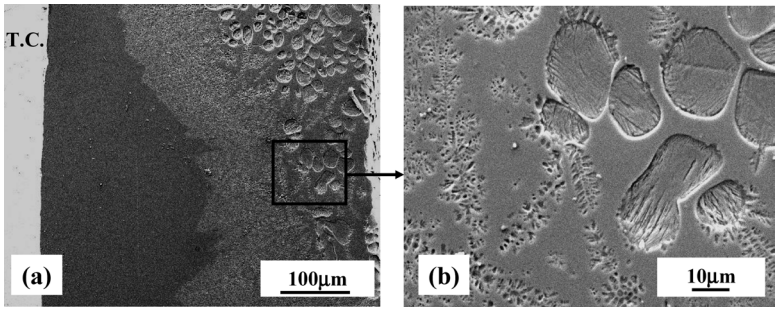

Fig. 7. SEM image of quenched slag (sample-4: C/S 1.5, 10 mass% Fe_tO, 5 mass% P_2O_5).

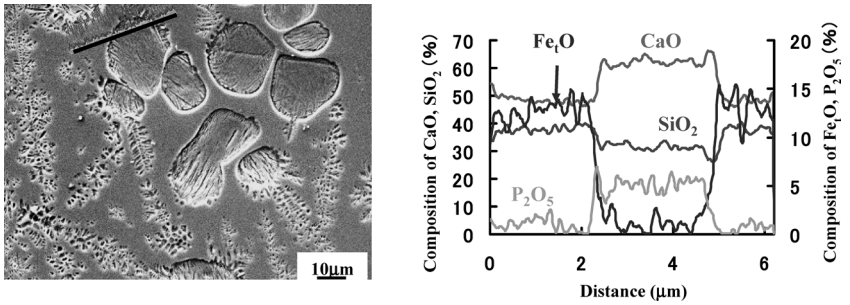

Fig. 8. SEM image and line scan of quenched slag (sample-4: C/S 1.5, 10 mass% Fe_tO, 5 mass% P_2O_5).

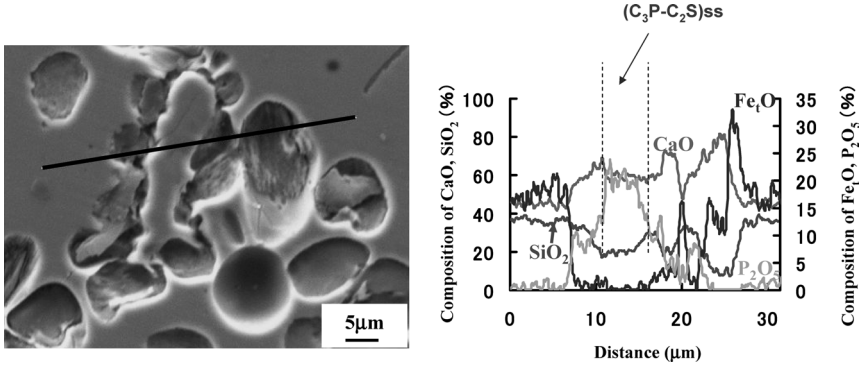

Fig. 9. SEM image and line scan of quenched slag (sample-5: C/S=1.5, 15 mass% Fe_tO, 5 mass% P_2O_5).

Those results show that although the concentrations of CaO and P_2O_5 were higher in the crystals, the concentration of Fe_tO was higher in the liquid phase (Fig. 8). Since the CaO concentration was twice as much as that of the SiO_2 in the crystal, the crystals are considered to be dicalcium silicate (C_2S). P_2O_5 diffused into the crystals when C_2S precipitated, unlike in the case of sample-1.

Figure 9 shows the EDS results of sample-5 (C/S=1.5, 15% Fe_tO). A crystal of irregular shape was observed in the center of the group of round crystals. From the EDS result, the concentration of CaO and P_2O_5 in the crystal was very high (59.2% CaO, 20.2% SiO_2, 20.2% P_2O_5, 0.3% Fe_tO). The crystal was identified as $8CaO–2.5SiO_2–P_2O_5$ ($C_3P–2.5C_2S$), a solid-solution between dicalcium silicate (C_2S) and calcium phosphate (C_3P). Thus, when the dicalcium silicate precipitated, the phosphorous included in the crystals reacted with CaO to form the solid solution in a very early stage of solidification.

Sample-6 (20% Fe_tO) did not show the crystallization. The details are also shown in the later section.

(3) Sample-7–9 (C/S=2.0, 10–20% Fe_tO, 5% P_2O_5)

The results of C/S=2, 10% Fe_tO (sample-7) are shown in **Fig. 10**. The crystals are bigger and the area of liquid phase is smaller than for sample-5. The grain size is about 22 μm.

From the line scanning results, where the center of the line scanning is the liquid phase between crystals, most Fe_tO exists in the liquid phase; the SiO_2 concentration difference between the crystal and liquid phases is small. The concentrations of CaO, P_2O_5 and SiO_2 were higher in the crystals, and since the concentration of CaO was twice as much as that of the SiO_2, the crystals were considered to be dicalcium silicate. Phosphorous was also included in the crystals when the C_2S precipitated.

As shown in **Fig. 11** (sample-9, C/S=2.0, 20% Fe_tO), an irregular crystal was observed in the center of the group of round crystals. From the EDS results, the concentration of CaO and P_2O_5 in this crystal was very high (55.4% CaO, 7.2% SiO_2, 37.3% P_2O_5, 0.1% FeO). It was identified as a solid-solution of dicalcium silicate and calcium phosphate, close to $4CaO–0.5SiO_2–P_2O_5$ ($C_3P–0.5C_2S$).

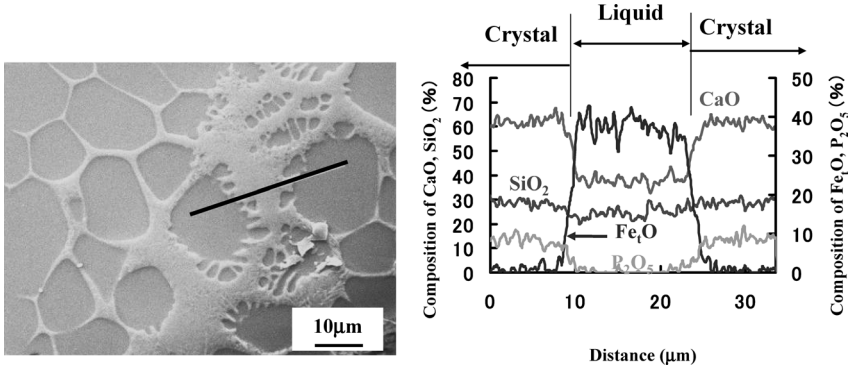

Fig. 10. SEM image and line scan of quenched slag (sample-7, C/S=2.0, 10 mass% Fe_tO, 5 mass% P_2O_5).

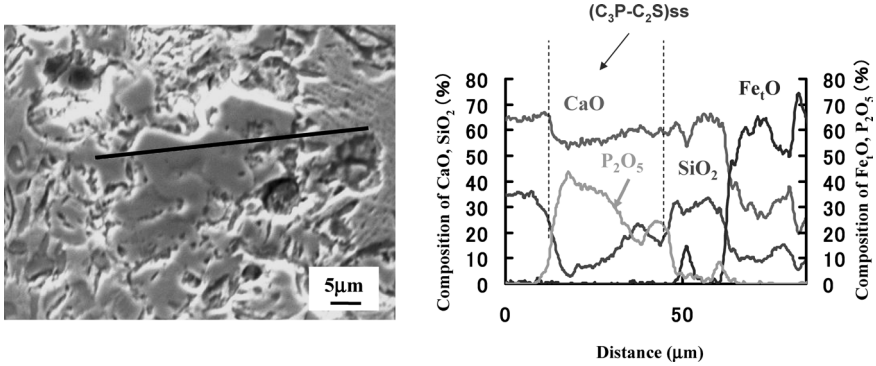

Fig. 11. SEM image and line scan of quenched slag (sample-9: C/S=2.0, 20 mass% Fe_tO, 5 mass% P_2O_5).

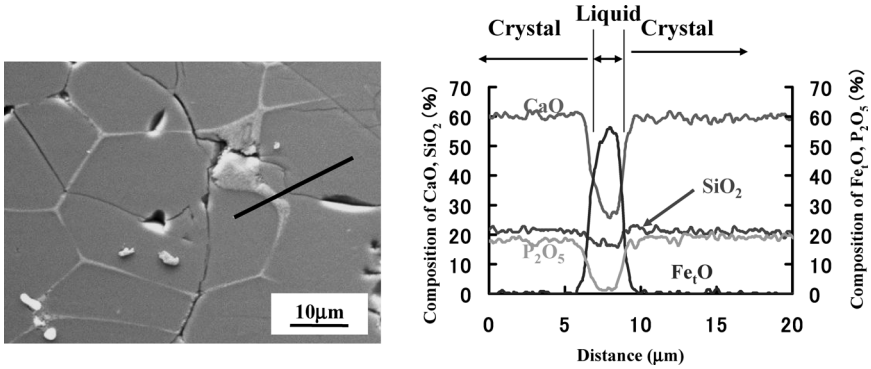

Fig. 12. SEM image and line scan of quenched slag (sample-10: C/S=2.5, 10 mass% Fe_tO, 5 mass% P_2O_5).

(4) Sample-10–12 (C/S=2.5, 10–20% Fe_tO, 5% P_2O_5)

In the C/S=2.5, 10% FeO slag (sample-10), crystals were bigger and the liquid area was smaller (**Fig. 12**). From the EDS results, the basicity of the crystal was about 2.6. The concentration of P_2O_5 in the crystal was very high (17.6%), and in liquid phase was 1.6%. A melt of low viscosity was formed, which might enhance crystal growth.

As shown in **Fig. 13**(a) (sample-12, C/S=2.5, 20% Fe_tO), an irregular crystal was observed in the center of the group of round samples. From the EDS results, the concentration of CaO and P_2O_5 in the crystal is very high (58.0% CaO, 18.7% SiO_2, 22.7% P_2O_5, 0.6% FeO). The crystal was identified as a solid-solution of dicalcium silicate and calcium phosphate, close to $7CaO–2SiO_2–P_2O_5$ ($C_3P–2C_2S$). In the other area, a solid-solution of dicalcium silicate and calcium phosphate was observed to be close to $4.6CaO–0.8SiO_2–P_2O_5$ ($C_3P–0.8C_2S$) (Fig. 13(b)).

3.2. The Relationship between Diameters of Crystals and Basicity

From the results of SEM observation, the crystal diameters were measured. The relationships among basicity, Fe_tO content and crystal diameter are shown in **Fig. 14**. The diameter increases with the increase in basicity and decreases with the increase in Fe_tO content. Since the increase in basicity leads to an increase in the amount of CaO, bigger crystals form. In the case of high Fe_tO content, the amount of liquid phase (calcium ferrite) increases and the crystals size decreases.

In Fig. 14, the regions of glassy and a solid solution between $C_2S–C_3P$ are also shown. In the slags of 20% Fe_tO for which the value of C/S is less than 2.0 (C/S<2.0, sample-3 and sample-6), no crystals were observed, it is a glassy area. From the quaternary phase diagram of the $CaO–SiO_2–FeO–P_2O_5$ system (20% Fe_tO), the melting

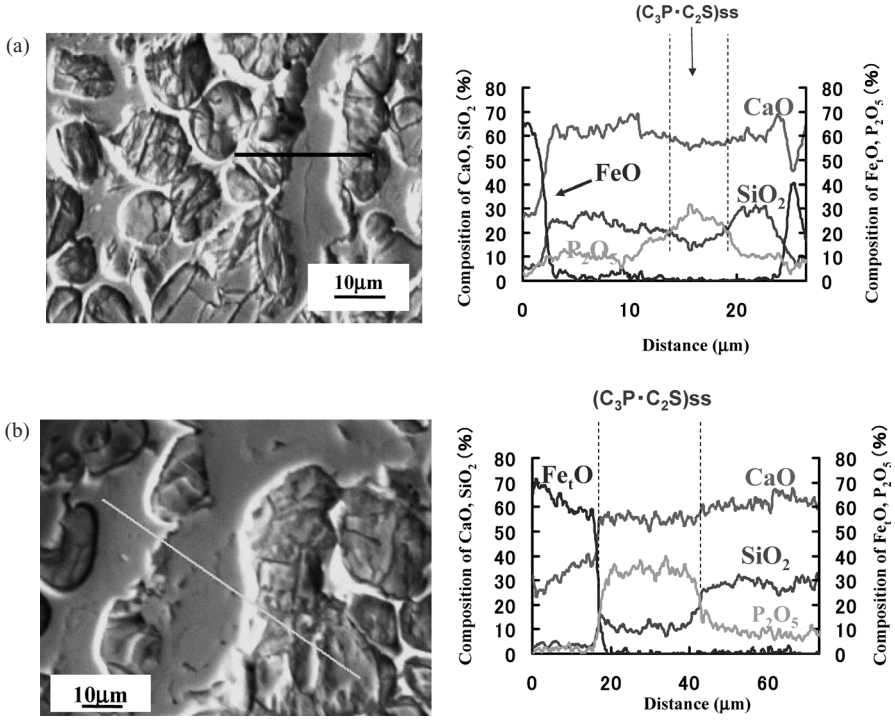

Fig. 13. SEM image and line scan of quenched slag (sample-12: C/S=2.5, 20 mass% Fe_tO, 5 mass% P_2O_5).

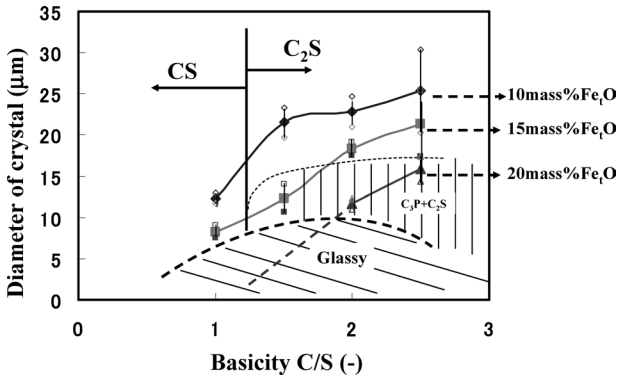

Fig. 14. Relationship between basicity of slag and diameter of crystal.

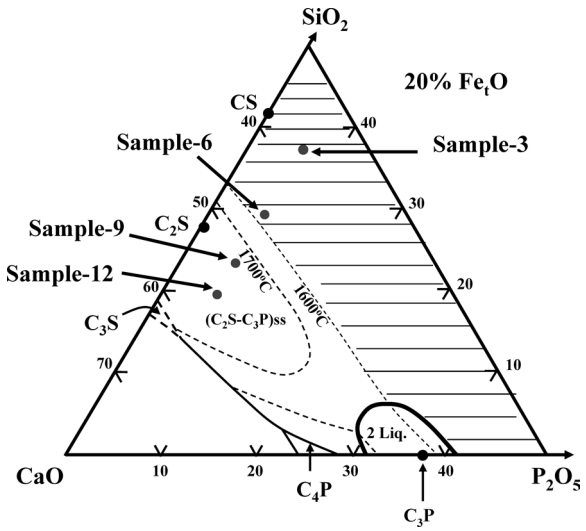

Fig. 15. Phase diagram of CaO–SiO_2–FeO–P_2O_5 system (FeO 20%).[12]

points of sample-3 and sample-6 are less than 1 600°C (**Fig. 15**).[12] As these powder samples were completely melted before quenching, a glassy phase could form under rapid quenching conditions (400 K/s).

In the case of high basicity and high FeO slags, a region of solid solution between dicalcium silicate and calcium phosphate exists. The solid solutions were always observed in the center of the group of C_2S crystals. Those crystals are considered to have precipitated in a very short time after solidification. When the viscosity of melt in the high-Fe_tO content was low, C_2S crystal with high phosphorous concentrations could easily gathered and so the precipitation of solid solution (C_2S–C_3P) might have occurred in an early stage of solidification.

3.3. Phase Separation at Initial Stage of Melting (Non-equilibrium State)

The compositions of liquids and crystals in the initial stage are plotted in a CaO–SiO_2–Fe_tO phase diagram (**Figs. 16** and **17**).

In Fig. 16(a), the initial crystal composition located in the region of primary crystalline phase region of CS. The liquid composition corresponded to the liquidus at 1 400°C, extrapolating from the composition of CS to the initial composition for 10% Fe_tO slag (sample-1). In the case of 15% Fe_tO slag, the composition of the liquid phase located in the Rankinite region (about 1 250°C). The compositions of the both crystals coincided with the one of CS. As mentioned above, 20% Fe_tO slag (sample-3) has a low melting point and shows a glassy phase.

When the basicity increased to 1.5, the crystal compositions located near the region of C_2S, and the compositions of liquid located at the same liquidus (1 400°C) as those of sample-1 and 2 (Fig. 16(b)). The positions of the liquids for 10% and 15% Fe_tO slag were not in the line extrapolating

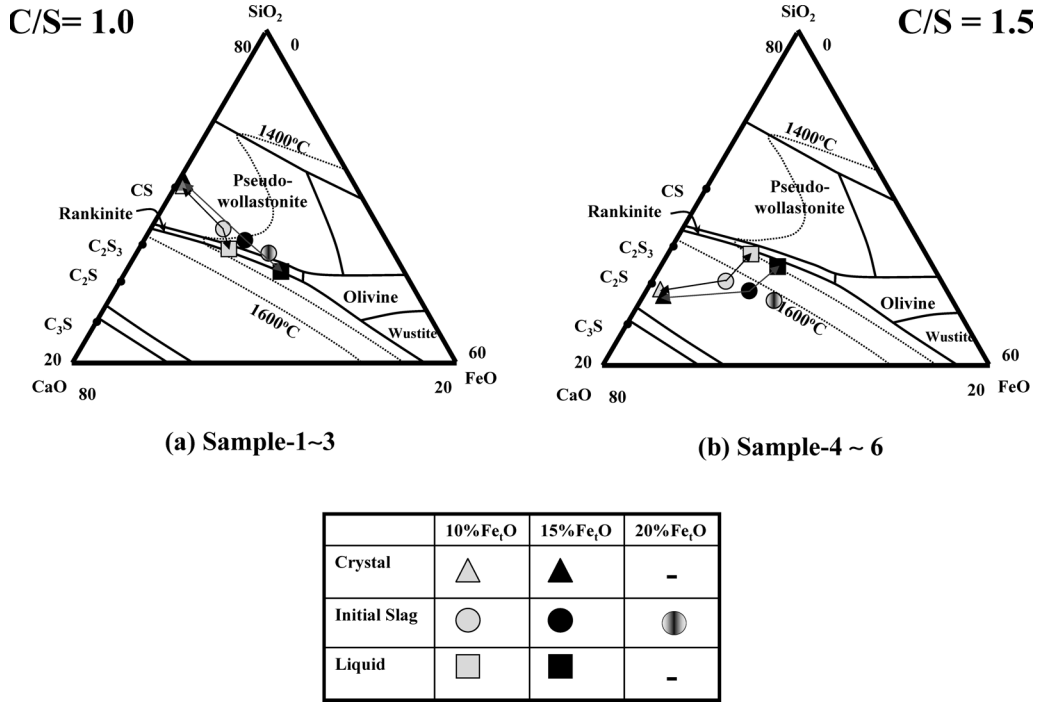

Fig. 16. Position of liquid and crystals precipitated from each samples.

from C_2S to the initial composition. This indicates that these samples did not achieve equilibrium. The rate of C_2S precipitation was quite fast, and so the Fe_tO diffusion from bulk would have been late. Then, Fe_tO content around the crystals could be lower in comparison to the equilibrium composition.

In Fig. 17(a), the liquid compositions located near the liquidus of 1 500 and 1 600°C. As the basicity is 2.0, the slag melting points are higher than 1 600°C. Although the melting temperature was lower than the melting point of an average chemical composition, the sample could be melted by the reaction heat among the mixed sample (The melted sample might not be a complete liquid phase and some solid phase already precipitated). As the melting point of 20% Fe_tO slag was lower than those of the other slags, the liquid composition located on the straight line extrapolating from the point of C_2S to initial composition.

In the case of the sample-10, C/S=2.5, 10% Fe_tO the precipitated crystal was close to C_3S, while those of the other two slags (15% Fe_tO and 20% Fe_tO) were close to C_2S, as shown in Fig. 17(b). The melting points of these three slags were over 1 900°C, whereas the experiment temperature for melting was 1 600°C. Actually pre-melted slag did not melt; however, the mixed samples seemed to melt instantaneously before the temperature reached to 1 600°C. As mentioned above, this was caused by the reaction heat. The enthalpies of reaction for CS, C_2S and C_3S almost the same and about −21 kcal (Eqs. (1)–(3)).

The reactions are expressed as follows:

$$CS: CaO(s)+SiO_2(s)=CaO\cdot SiO_2(s)$$
$$\Delta H^\circ=-20.7\,\text{kcal (at 1 600°C)}.....(1)$$

$$C_2S: 2CaO(s)+SiO_2(s)=2CaO\cdot SiO_2(s)$$
$$\Delta H^\circ=-21.5\,\text{kcal (at 1 600°C)}.....(2)$$

$$C_3S: 3CaO(s)+SiO_2(s)=3CaO\cdot SiO_2(s)$$
$$\Delta H^\circ=-21.0\,\text{kcal (at 1 600°C)}.....(3)$$

Because of these reaction heats, the mixed sample could be melted even if the measure temperature was only 1 600°C. And because of the formation of CS, C_2S and C_3S, the melted sample would be the state of coexistence of solid and liquid. For example, if we assumed that the only one crystal such as $2CaO\cdot SiO_2$ was precipitated, the following reaction could be considered at the instance of the melting and the start of solidification. In the Eq. (5), the liquids and the precipitated crystal (C_2S) coexist. Furthermore, the temperatures for sample-7 and sample-10 are estimated to 1 978°C and 1 940°C, respectively, from the adiabatic calculations in assumption with the initial temperature of 1 600C.

$$2CaO(s)+SiO_2(s)=2CaO\cdot SiO_2(s)-\Delta H^\circ .....(4)$$
$$\downarrow$$
$$2CaO(l)+SiO_2(l)=2CaO\cdot SiO_2(s)-\Delta H^\circ .....(5)$$

In the case of two samples (sample-11, 12), the position of the liquid composition deviated from the straight line (equilibrium point) toward the low-temperature region.

Although the sample-10 seems to be in the equilibrium phase separation among the initial composition, the precipitated crystal (C_3P) and the formed liquid, actually P_2O_5 in the crystal was relatively high and about 18%. The crystal precipitated in the sample-10 will be a solid solution between C_2S and C_3P ($(C_2S–C_3P)_{SS}$) as shown in Fig. 17(c).

The solid solution itself, which precipitated in the center of the round C_2S crystals, was not homogeneous. **Figure 18** shows the results of the line scan inside the solid solution. The average concentrations within the two line scans are shown in **Table 2**. Although the content of Fe_tO was very low in both, the content of P_2O_5 and SiO_2 were quite differ-

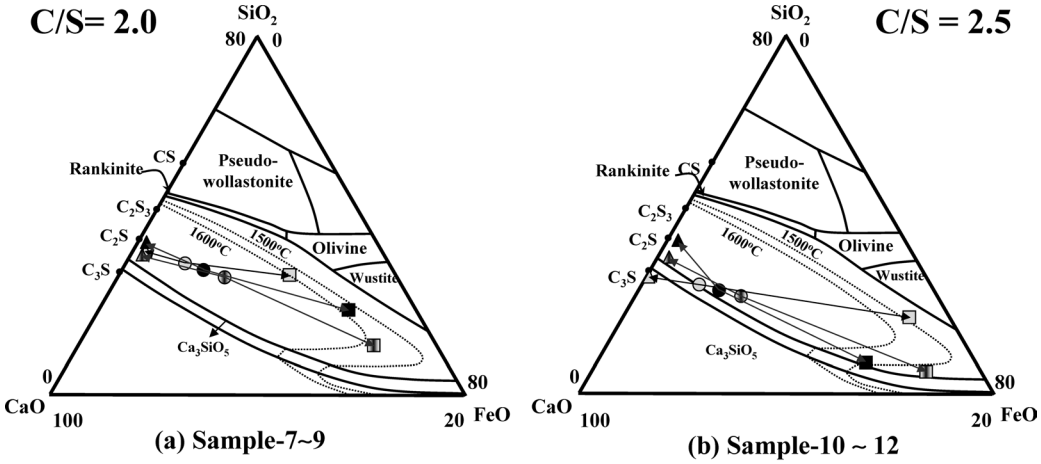

	10%Fe_tO	15%Fe_tO	20%Fe_tO
Crystal	△	▲	◭
Initial Slag	○	●	◑
Liquid	□	■	◨

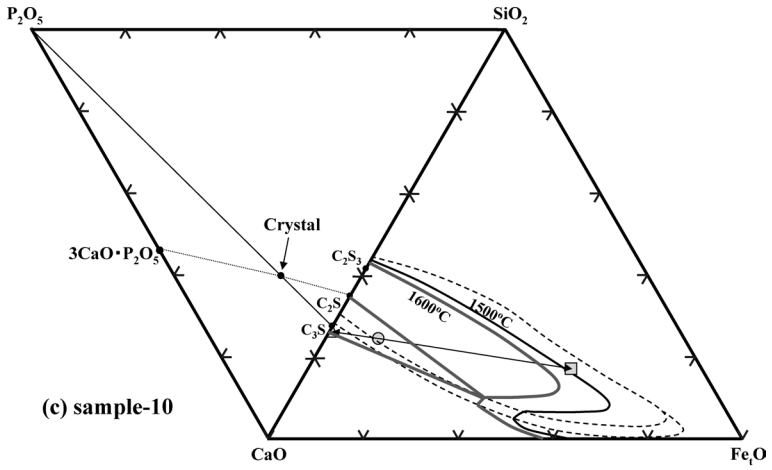

Crystal composition				
SiO_2	CaO	P_2O_5	Fe_tO	C_3P·2(C_2S)
21.5%	60.3%	17.9%	0.29%	

Fig. 17. Position of liquid and crystals precipitated from each samples.

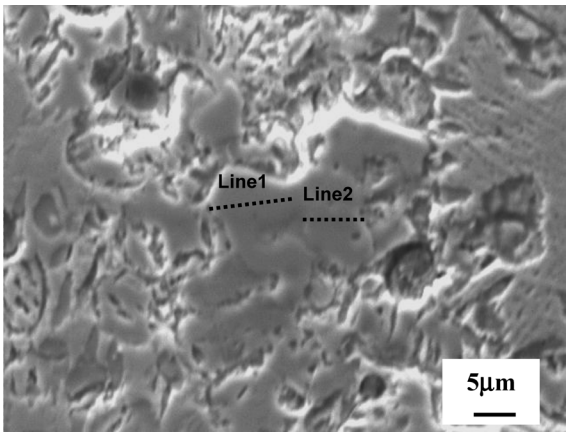

Fig. 18. Results of EDS analysis in the solid solution (sample-9: C/S=2.0, 20 mass% Fe_tO, 5 mass% P_2O_5).

Table 2. Average compositions in the line scan (mass%).

	CaO	SiO_2	P_2O_5	Fe_tO	Solid solution
Line 1	55.4	7.1	37.2	0.1	C_3P-0.5C_2S
Line 2	58.3	14.6	26.9	0.2	C_3P-1.3C_2S

ent. The compositions of the solid solution were C_3P–0.5C_2S and C_3P–1.3C_2S, respectively.

3.4. The Relationship among the Phosphorous Distribution, Basicity and Fe_tO Content

From the content of P_2O_5 in the crystals and liquids, Lp ($=(P_2O_5)_{cry}/(P_2O_5)_{liq}$) can be calculated. **Figure 19** shows the relationship between Lp and basicity.

In the C/S=1 slag, P_2O_5 did not exist in the crystal and Lp was close to 0. Figures 19(a) and 19(b) show the variations of Lp (for the single crystal and the solid solution, re-

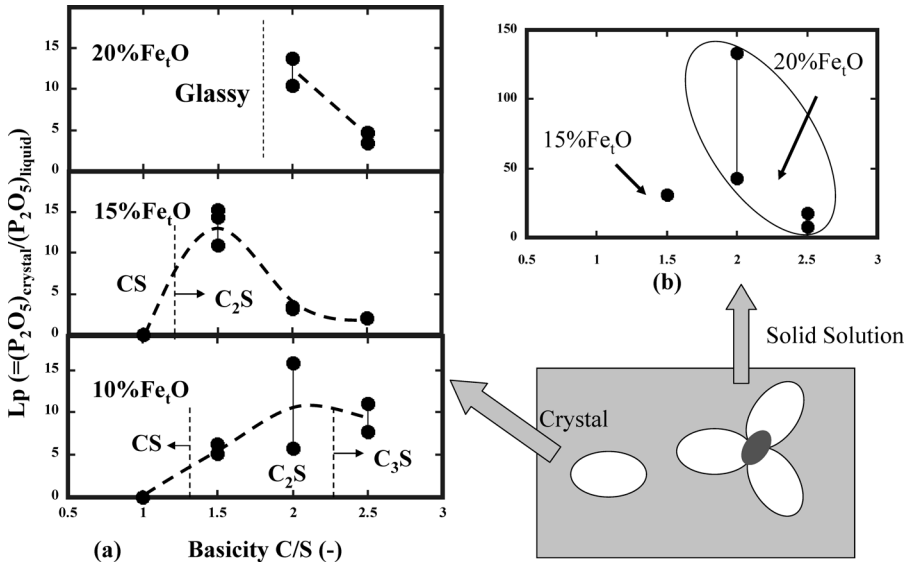

Fig. 19. Relationship between basicity of slag and phosphorous distribution between crystal and liquid.

spectively) in terms of basicity and Fe_tO content. In the case of 10% Fe_tO, the Lp value increased with the increasing of basicity to a maximum point at 2.0. On the other hand, the maximum point in 15% Fe_tO was 1.5 and the one in 20% Fe_tO was 2.0. However, as the region in low C/S, less than 1.5, for 20% Fe_tO showed a glassy phase, the maximum Lp would probably exist around a C/S of 1.5 when a crystal precipitated under a slow cooling rate.

When the solid solution precipitated, the value of Lp became very high as shown in Fig. 19(b). The maximum value of Lp ranged from 50 to 140 around C/S=2.0. This result supports the current actual operations involving high Fe_tO content slag.

4. Conclusions

Using Hot-Thermocouple Technique, the samples were melted and quenched quickly. The crystallization behavior was investigated by SEM and EDS. The results are as follows:

(1) A sample with a low melting point can be melted completely and, upon quenching shows a glassy phase. Meanwhile, for a high melting point sample, crystallization starts just after melting. The high melting point sample can be melted with reaction heat to form CS, C_2S and C_3S. In these cases, the crystallization starts at almost the same time as the melting.

(2) The crystal diameters increase with the increase of basicity and the decrease of Fe_tO concentration.

(3) Lp ($=(P_2O_5)_{cry}/(P_2O_5)_{liq}$) shows a maximum value around 5 to 15 in the region of C_2S for 10%Fe_tO. On the other hand, Lp of 15% Fe_tO samples is maximized at C/S=1.5. In the case of 20% Fe_tO, Lp reaches a maximum at C/S=2.0.

(4) When the solid solution, C_2S–C_3P precipitates, Lp drastically increases to 40 in the sample (20% Fe_tO, C/S=2.0).

Acknowledgements

This study has been carried out by the support of the Research Group of "New refining process by using multiphase fluxes" in ISIJ. The authors gratefully thank Prof. F. Tsukihashi, the University of Tokyo, a director of the Research Group and all the members for their helpful suggestions and novel discussions.

REFERENCES

1) T. Hamano, M. Horibe and K. Ito: *ISIJ Int.*, **44** (2004), 263.
2) T. Hamano, H. Tamai and K. Ito: *CAM-ISIJ*, **14** (2001), 121.
3) M. Matsushima, S. Yadoomaru, K. Mori and Y. Kawai: *Tetsu-to-Hagané*, **62** (1976), 182.
4) K. Ito, M. Yanagisawa and N. Sano: *Tetsu-to-Hagané*, **68** (1982), 342.
5) R. Inoue and H. Suito: *ISIJ Int.*, **46** (2006), 174.
6) R. Inoue and H. Suito: *ISIJ Int.*, **46** (2006), 180.
7) R. Inoue and H. Suito: *ISIJ Int.*, **46** (2006), 188.
8) T. Hamano, S. Fukagai and F. Tsukihashi: *ISIJ Int.*, **46** (2006), 490.
9) E. M. Levin, C. R. Robbins and H. F. McMurdie: Phase Diagrams of Ceramists, Vol. 1, The American Ceramic Society, Westerbille, OH, (1964), 204.
10) Y. Kashiwaya, C. E. Cicutti, A. W. Cramb and K. Ishii: *ISIJ Int.*, **38** (1998), 348.
11) Y. Kashiwaya, C. E. Cicutti and A. W. Cramb: *ISIJ Int.*, **38** (1998), 357.
12) R. S. Roth, T. Negas and L. P. Cook: Phase Diagrams for Ceramists, Vol. 4, The American Ceramic Society, Westerbille, OH, (1981), 209.

Appendix

In the present study, the quantitative analysis was carried out using EDS analysis. The polished samples were coated by Au evaporation, mainly before observation; some samples were coated by carbon evaporation. Since the reliability of the EDS analyses is not high, the data from EDS analyses were corrected by EPMA analysis. Comparison of the results between EDS and EPMA analysis for the concentration of P_2O_5, CaO and SiO_2 are shown in **Figs. A1**, **A2** and **A3**, respectively. The coating of the sample for EPMA analysis was carried out by carbon under the same conditions as for the one used in EDS analysis.

The differences between the results of EDS and EPMA

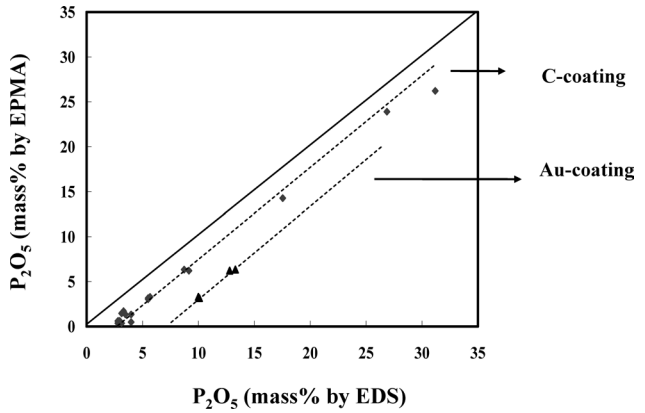

Fig. A1. Comparison of the P_2O_5 concentration measured by EPMA and EDS.

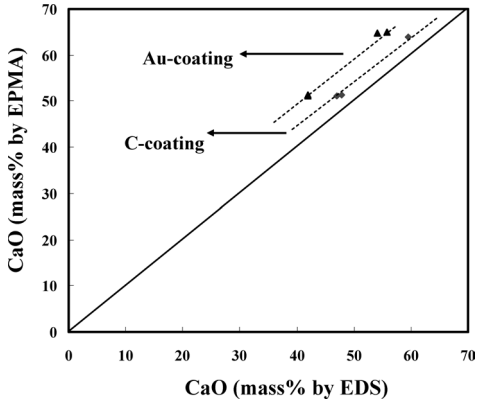

Fig. A2. Comparison of the CaO concentration measured by EPMA and EDS.

varied by element. Phosphorous content by EDS was higher than that of EPMA for both the gold coating and the carbon coating. Since the energy for the characteristic X-ray, Kα, of P is 2.014 keV, which overlaps with the Mα of Au (2.121 keV), the value of the Au coating always shows the higher one (Fig. A1). On the other hand, CaO content as evaluated by EDS was lower, as shown by Fig. A2. Also, the SiO_2 content was a little higher, as shown by Fig. A3. However, the linearity of the results of EDS is the same as those of EPMA. The data from EDS analysis was corrected using a simple linear regression equation.

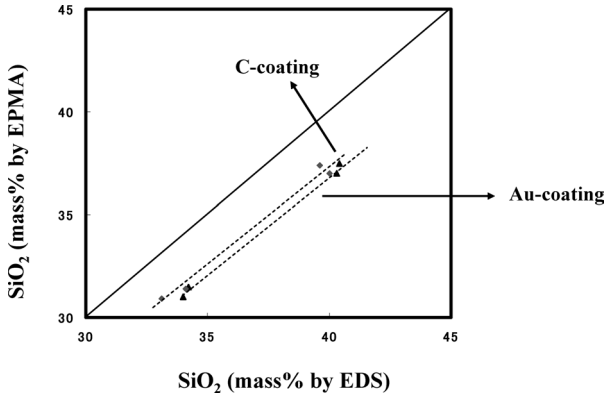

Fig. A3. Comparison of the SiO_2 concentration measured by EPMA and EDS.